Binding, Proteolytic, and Crystallographic Analyses of Mutations at the Protease−Inhibitor Interface of the Subtilisin BPN′/Chymotrypsin Inhibitor 2 Complex[†,‡]

Evette S. Radisky, Gene Kwan,[§] Chia-Jung Karen Lu, and Daniel E. Koshland, Jr.*

Department of Molecular and Cell Biology, University of California, Berkeley, California 94720

Received June 9, 2004; Revised Manuscript Received August 23, 2004

ABSTRACT: A series of mutants of chymotrypsin inhibitor 2 (CI2), at residues that interact with the inhibited enzyme subtilisin BPN′, were studied to determine the relative importance of intermolecular contacts on either side of the scissile bond. Mutants were tested for inhibition of subtilisin, rates of hydrolysis by subtilisin, and ability to acylate subtilisin. Additionally, crystal structures of the mutant CI2 complexes with subtilisin were obtained. Ordered water molecules were found to play an important role in inhibitor recognition, and features of the crystal structures, in combination with biochemical data, support a transition-state stabilization role for the P_1 residue in subtilisin catalysis. Consistent with the proposed mechanism of inhibition, in which rapid acylation is followed by religation, leaving-group contacts with the enzyme were found to be more critical determinants of inhibition than acylating-group contacts in the mutants studied here.

The protein inhibitors of serine proteases inhibit enzymes by binding extremely tightly at the enzyme active site yet resisting proteolysis (*1*, *2*). Using the subtilisin/chymotrypsin inhibitor 2 (CI2)[1] complex as a model, we have previously presented evidence (*3*) that these inhibitors form acyl−enzyme intermediates rapidly with target enzymes, but the inhibitor rapidly religates, in preference to the forward reaction of hydrolytic deacylation. In Scheme 1, k_{-2} is much greater than k_3, resulting in an apparent equilibrium between the Michaelis complex and the acyl−enzyme. We have termed this rapid religation phenomenon, in which the tight and oriented binding of the leaving-group peptide (H_2N-R' in Scheme 1) prevents acyl−enzyme hydrolysis and favors the reverse reaction, the clogged gutter mechanism (*3*).

On the basis of this mechanism, in which inhibition is caused by the very slow rate-limiting step of deacylation and product release, we would predict that those interactions between the enzyme and inhibitor involving the leaving-group R′ fragment of CI2 would be particularly critical. With good substrates of subtilisin, acylation is typically rate-limiting (*4*, *5*), and substrate specificity and reaction rates are largely determined by contacts between the enzyme and the acylating R portion of the substrate, most notably the P_1 residue[2] (*6*, *7*). In contrast, for inhibitors that act by the clogged gutter mechanism, interactions between the enzyme and P_1 residue are predicted to be comparatively less important for inhibitor hydrolysis than those interactions with R′ residues that promote leaving-group retention in the active site.

Scheme 1: Mechanism of CI2 Cleavage by Subtilisin[a]

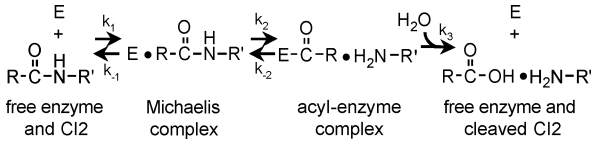

[a] Subtilisin is represented by E, and CI2 is depicted as N- and C-terminal protein fragments R and R′, respectively, connected by the scissile peptide bond targeted by the enzyme.

To expand our understanding of this mechanism of inhibition, we examined the details of intermolecular interactions between CI2 and subtilisin BPN′. We began by examining the time frame of acylation, showing that, for the initial reaction (k_2 in Scheme 1), CI2 is comparable to a good substrate and hence that the deacylation reaction is solely

[†] This work was supported in part by a National Institutes of Health Grant DK09765 (to D.E.K.), and E.S.R. was supported by a National Institutes of Health postdoctoral fellowship. The Advanced Light Source is supported by the Director, Office of Science, Office of Basic Energy Sciences, Materials Sciences Division of the U.S. Department of Energy under contract no. DE-AC03-76SF00098 at the Lawrence Berkeley National Laboratory.

[‡] Structure coordinates have been deposited in the Protein Data Bank.

* To whom correspondence should be addressed. E-mail: dek@uclink.berkeley.edu. Phone: (510) 642-0416. Fax: (510) 643-6386.

[§] Present address: UCSD School of Medicine, La Jolla, CA 92093.

[1] Abbreviations: CI2, chymotrypsin inhibitor 2; PCR, polymerase chain reaction; HPLC, high-pressure liquid chromatography; SDS, sodium dodecyl sulfate; PAGE, polyacrylamide gel electrophoresis; DTT, dithiothreitol; TFA, trifluoroacetic acid; PEG, poly(ethylene glycol); CHES, 2-[*N*-cyclohexylamino]ethanesulfonic acid; CCD, charge-couple device; PDB, Protein Data Bank; BPTI, bovine pancreatic trypsin inhibitor; OMTKY3, turkey ovomucoid third domain. CI2 mutant nomenclature is according to the following example, using the single letter amino acid code: M59A refers to residue 59, formerly methionine, now mutated to alanine.

[2] Throughout the text, we use the nomenclature of Schechter and Berger (*35*) for designating substrate residues surrounding the cleavage site and the corresponding binding subsites on the enzyme. Starting at the scissile bond, substrate residues are numbered P_1, P_2, P_3, etc. in the direction of the N terminus and P_1', P_2', P_3', etc. in the direction of the C terminus. The corresponding enzyme subsite binding pockets are numbered S_1, S_2, etc.

10.1021/bi048797k CCC: $27.50
Published on Web 10/05/2004

responsible for the proteolytic resistance of the inhibitor. Next, we systematically mutated residues of CI2 at the binding interface that make substantial contacts with the enzyme. On the acylating R side of the scissile bond, we chose the P_1 Met 59 residue of CI2, which immediately precedes the cleavage point and binds in the S_1 primary specificity subsite of subtilisin, as the main target of study. The CI2 P_1 residue was mutated to Phe and Tyr, which are the most preferred P_1 residues for subtilisin (*7*−*9*), Lys, which is proposed to form stabilizing electrostatic interactions with the enzyme (*10*, *11*), and Ala and Gly, which remove large hydrophobic side-chain contacts and potentially allow greater backbone mobility. On the leaving group R′ side of the scissile bond, the P_2' residue Tyr 61 shows the closest association with the enzyme, forming an aromatic ring stacking interaction with Phe 189 of subtilisin (*12*); accordingly, Tyr 61 of CI2 was mutated to Ala, altering these favorable contacts. The native and mutant complexes were compared with respect to binding affinities, rates of cleavage, and ability to form the acyl−enzyme. Additionally, crystal structures of the complexes were analyzed to determine whether the observed functional effects arise solely from the loss of the targeted intermolecular interactions and whether the scissile bond is still optimally oriented for acylation in the mutant complexes.

EXPERIMENTAL PROCEDURES

Subtilisin BPN′. Recombinant subtilisin BPN′ (*13*), modified by the addition of a C-terminal 6-His tag (*3*), was prepared as described previously (*14*). Active enzyme concentrations were determined by kinetic assay with succinyl-Ala-Ala-Pro-Phe-*p*-nitroanilide as described previously (*14*).

CI2. Truncated recombinant CI2 (*3*, *14*) was expressed and purified from *Escherichia coli* as described previously (*14*). Throughout the text, we use the amino acid numbering of the original full-length protein sequence. The CI2 expression construct was mutagenized using the PCR-based QuikChange method (Stratagene), and the mutant expression constructs were verified by DNA sequencing. Mutant CI2 proteins were expressed and purified following the same protocols used for the wild-type inhibitor (*14*). Wild-type and mutant CI2 concentrations were determined by peak integration from HPLC absorbance traces and by titration with subtilisin BPN′ of a known concentration, as described previously (*14*).

Subtilisin Inhibition (Binding) Studies. CI2 is a potent slow, tight-binding inhibitor of subtilisin (*15*). Inhibition constants K_i were calculated from the reduced rates of subtilisin hydrolysis of a chromogenic substrate, succinyl-Ala-Ala-Pro-Phe-*p*-nitroanilide, in the presence of wild-type or mutant CI2 [all assay conditions, procedures, equations, and analysis are described in detail elsewhere (*14*)]. K_i values reported represent mean values from two or more experiments.

Hydrolysis Studies. The initial linear rate of depletion of intact CI2 in time-course incubations with subtilisin BPN′ was monitored by HPLC, as described previously (*14*). For each time point, HPLC injections were performed in duplicate, and remaining CI2 quantities were determined by peak integration of absorbance traces and comparison to standard curves generated from known quantities of pure CI2 (*14*).

SDS−PAGE of Acyl−Enzyme Complexes. Subtilisin BPN′ (1−8 μg) was incubated with a molar excess of each CI2 variant (3−10 μg) in 100 mM Tris at pH 8.6, on ice for 15 min, to allow formation of an apparent equilibrium mixture of the noncovalent complex and the acyl−enzyme species. Samples were acidified to pH 1 to inactivate subtilisin prior to denaturation by heating in a loading buffer. SDS gels (15% acrylamide) were run under standard conditions using a Bio-Rad Minigel apparatus and Coomassie-stained using standard procedures. A homemade molecular weight marker, in which the protein standards were present in varying amounts ranging from 0.05 to 1 μg, was used to quantify the acyl−enzyme band by comparison, using a Kodak Digital Science DC40 camera and Kodak Digital Science 1D electrophoresis documentation and analysis software.

Rapid Quench Observation of Acyl−Enzyme Formation. Reactions were run in a Bio-Logic SFM-400/Q four-syringe quench-flow instrument, configured with no additional delay lines between the mixers and equipped with a circulating water bath to control the temperature of the reactants. Syringe 1 contained subtilisin BPN′ (14 μM in 10 mM NH_4OAc at pH 5.8 and 1 mM DTT); syringe 2 contained buffer (50 mM NH_4HCO_3 at pH 8.6); syringe 3 contained CI2 (28 μM in 25 mM NH_4HCO_3 at pH 8.6); and syringe 4 contained quench solution (0.8% TFA). Reactions took place at 25 °C in the 22 μL intermixer volume between mixers 2 and 3, with the reaction times determined by the flow rate, and the enzyme was effectively quenched by acidification to pH 1 after mixing with the TFA quench solution at mixer 3. Reactions after mixing contained 3.5 μM subtilisin and 14 μM CI2 prior to quenching, and reaction times ranged from 2.75 to 82.5 ms. Quenched reaction volumes were collected, immediately frozen on dry ice, lyophilized, and then redissolved in gel-loading buffer and analyzed by SDS−PAGE as described above.

Crystallization. Crystals of the mutant complexes failed to form under the conditions used previously to grow crystals of the native complex in space group $P2_12_12_1$ (*3*). A broad screen of crystallization conditions identified a robust protocol that yielded good diffraction quality crystals for all CI2 variant complexes, with only minor customization of conditions for each variant. Crystals of the native complex were grown as well under these new conditions. Lyophilized subtilisin BPN′ and CI2 were each dissolved in 10 mM NaOAc (pH 5.8) and mixed in a 1:1.2 stoichiometric molar ratio; the ideal total protein concentration varied among the CI2 mutants. Crystals were grown at 4 °C in hanging drops over a reservoir of 0.1 M sodium citrate (pH 4.6), 20% 2-propanol, and 15% PEG; the optimal molecular weight of PEG varied among the CI2 mutants. Crystal drops were prepared by mixing 2 μL of the protein solution with 2 μL from the reservoir or, in some cases, 5 μL of the protein solution with 5 μL from the reservoir; some CI2 variants required an additional additive to the drop to achieve the best possible crystal diffraction quality. Customizations of the protocol for individual CI2 variants are as follows: the wild-type and M59K CI2 complexes were grown in PEG 4000, with 4 mg/mL total protein concentration and 3% xylitol added to the crystallization drops; the M59F and Y61A CI2 complexes were grown in PEG 400, with 5 mg/mL total protein concentration; the M59G CI2 complex was grown in PEG 400, with 3 mg/mL total protein concentration; the M59A CI2 complex was grown in PEG monomethyl ether 750, with 5 mg/mL total protein concentration;

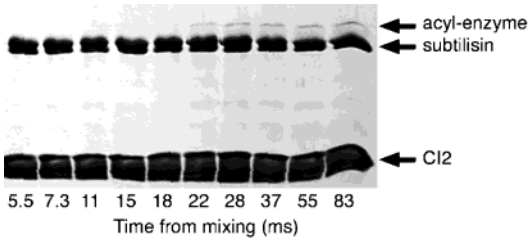

FIGURE 1: Demonstration of the rapid acylation of subtilisin by CI2. Subtilisin BPN′ and CI2 were mixed in a stop-quench instrument and then quenched with acid, inactivating the enzyme and trapping the acyl−enzyme, after varying mixing times. The quenched samples were analyzed by SDS−PAGE.

and the M59Y CI2 complex was grown in PEG 750 monomethyl ether, with 4 mg/mL total protein concentration. Crystals were rod-shaped with hexagonal cross sections and belonged to space group $P6_522$. Crystals were briefly transferred to a cryoprotectant solution, containing 0.1 M sodium citrate (pH 4.6), 15% 2-propanol, 15% PEG 2000, and 20% PEG 400, and then were flash-frozen in liquid N_2. For crystals subjected to a pH jump, the cryoprotectant solution contained 0.1 M CHES (pH 9.0), 15% 2-propanol, 15% PEG 2000, and 20% PEG 400.

Crystal Data Collection and Processing. For each variant CI2 complex, synchrotron X-ray data were collected from a single crystal at 100 K using an ADSC Quantum 210 CCD detector at Advanced Light Source beamline 5.0.1 or 8.3.1, Lawrence Berkeley National Laboratory. The automation package ELVES (*16*) was used to direct MOLFLM (*17*), for indexing and integration, and SCALA (*18*), for scaling and merging the reflections. The M59K CI2 complex was the first to yield diffraction quality crystals under the described crystallization conditions, and the M59K CI2 complex structure was solved by molecular replacement using EPMR (*19*), using as the search model the wild-type CI2/subtilisin complex in space group $P2_12_12_1$ (PDB ID 1LW6), with solvent molecules omitted (*3*). A test set comprised of 5% of the total reflections, assigned at random, was excluded from refinement to allow calculation of the free *R* factor. The model was improved through alternating cycles of manual rebuilding using the interactive graphics program O (*20*), automated refinement using REFMAC5 (*21*), and automated solvent addition using ARP/WARP (*22*). Structure refinement of the subsequent variant CI2 complexes used the near-finished structure of the M59K CI2 complex as a starting model and followed the same refinement protocol. The free *R* test sets for the subsequent variant CI2 complexes were inherited from the M59K CI2 complex. Model validation was carried out using PROCHECK (*18*) and WHATCHECK (*23*). Superpositions were performed using GEM (*24*).

RESULTS AND DISCUSSION

CI2 Mechanism of Inhibition. Although the protein protease inhibitors are often thought of as unreactive, we have previously shown that an acyl−enzyme species forms within the first minutes after mixing of CI2 and subtilisin BPN′ (*3*). We now show that the acyl−enzyme is detectable within milliseconds after mixing (Figure 1), and while our assay method is not quantitative enough to allow exact determination of an acylation rate constant (k_2 in Scheme 1), it is apparent from this illustration that CI2 falls into the category of excellent peptide substrates of subtilisin with respect to the acylation step. For comparison, the good peptide substrate succinyl-Ala-Ala-Pro-Phe-*p*-nitroanilide displays rate-limiting acylation with subtilisin BPN′ and is cleaved with a k_{cat} of 50 s^{-1}, equivalent to a turnover time of 0.02 s (*5*). For CI2, the subsequent deacylation and product release steps are not so facile, however, because the overall rate for turnover is 3.8×10^{-6} s^{-1}, equivalent to a turnover time of 3 days (*14*). The proportion of the enzyme present in the acylated form accumulates to represent only ~6% of the total, indicating that the back reaction of peptide religation (k_{-2} in Scheme 1) is rapid and that the Michaelis complex is favored over the acyl−enzyme in the resulting equilibrium (*3*). To understand how the attractive intermolecular binding forces on either side of the scissile bond contribute to this mechanism of inhibition, we analyzed six CI2 mutants, M59F, M59Y, M59K, M59A, M59G, and Y61A, with respect to inhibition constants with subtilisin, rates of hydrolysis by subtilisin, formation of an acyl−enzyme with subtilisin, and structural changes in the complexes with subtilisin.

Table 1: Effect of CI2 Mutations on Subtilisin BPN′ Inhibition and Hydrolysis

	inhibition		hydrolysis	
CI2 mutant	K_i (M)	relative	k_{cat} (s^{-1})	relative
wild type	3.0×10^{-12}	1	3.8×10^{-6}	1
M59G	1.3×10^{-10}	44	3.8×10^{-6}	1
M59A	1.7×10^{-11}	6	2.0×10^{-5}	5
M59K	1.9×10^{-11}	6	4.7×10^{-5}	12
M59Y	3.3×10^{-12}	1	8.5×10^{-6}	2
M59F	1.7×10^{-11}	6	1.7×10^{-5}	4
Y61A	4.6×10^{-10}	153	2.6×10^{-4}	67

Inhibition Constants, Hydrolysis Rates, and Acyl−Enzyme Formation of CI2 Mutant Complexes. The data from inhibition and hydrolysis studies with the CI2 mutants are presented in Table 1; we report K_i, equivalent to the dissociation constant K_d, and k_{cat}, the overall rate of turnover. We found that mutation of Tyr 61 has a substantially greater impact on CI2 function than mutation of Met 59, consistent with our prediction of the leaving-group importance in the mechanism of inhibition, and that the larger effect of the Tyr 61 mutation is manifest both through an increased inhibition constant, which reflects a decrease in binding affinity, and through an increased rate of enzymatic hydrolysis.

From the viewpoint of substrate specificity studies, which have generally shown P_1 and P_4 to be the most critical positions for subtilisin substrate recognition and attribute lesser importance to the leaving-group residues (*6*, *7*), the greater importance of the P_2' residue for both binding and hydrolysis of CI2 is surprising. However, this finding is fully consistent with our mechanism of inhibition. The rate-determining step in proteolysis of the inhibitor involves hydrolytic attack on the acyl−enzyme complex and product release (k_3 in Scheme 1). The consensus model of the serine protease reaction features the hydrolytic water molecule approaching the acyl−enzyme from the face where the leaving group (R′) has departed (*25*−*27*). In the subtilisin/CI2 acyl−enzyme, the newly formed R′ amino terminus must begin to dissociate from the enzyme surface to clear a path for the hydrolytic water molecule. In the wild-type CI2

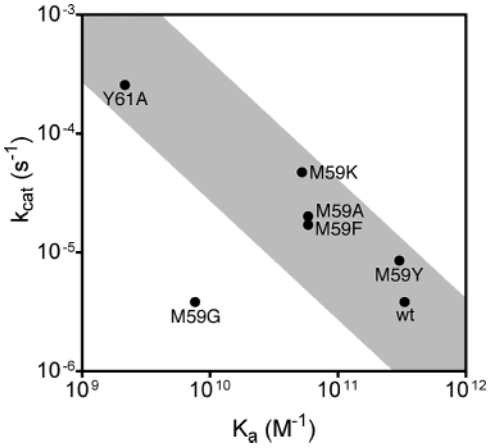

FIGURE 2: Binding/hydrolysis correlation. Hydrolysis rates k_{cat} are plotted versus association constants K_a, calculated as the reciprocal of inhibition (dissociation) constants K_i. Both axes are log-scaled.

complex, the interaction between CI2 Tyr 61 and subtilisin Phe 189 favors retention of the newly formed R′ amino terminus at the enzyme interface, and removal of this favorable interaction by mutation hastens departure of the R′ leaving group, accelerating turnover.

We found that the rate of CI2 hydrolysis correlates inversely with the binding affinity (Figure 2), a correlation consistent with the clogged gutter mechanism of inhibition, although it should be noted that the M59G mutant presents a striking exception to this trend. The rate-determining step in inhibitor turnover involves hydrolysis of the acyl−enzyme and subsequent product release. Hydrolysis requires at least partial dissociation of the R′ side of the CI2-binding loop, as discussed above, and product release requires full dissociation of both R and R′ sides of the cleaved binding loop. An inhibitor with optimal enzyme complementarity and strong binding affinity in the intact form will likely remain resistant to dissociation as the complex progresses through the acyl−enzyme to the cleaved form, hence, the observed correlation.

To determine whether any of the mutations studied had an appreciable effect on the ability of the complex to form an acyl−enzyme, subtilisin BPN′ was incubated with the variants of CI2 and then acid-quenched, trapping the equilibrium acyl−enzyme population for detection by gel analysis (Figure 3). The acyl−enzyme formation observed with wild-type CI2 was reproduced with the mutant inhibitors, which displayed between 2 and 10% of the acyl−enzyme species, as a proportion of the total enzyme. Again, however, the M59G mutant represents a major departure from the other mutants; no acyl−enzyme species was detected for M59G in any of four replicate assays.

Crystal Structures of the CI2 Mutant Complexes. To enable interpretation of the biochemical data for the CI2 mutants in terms of the loss of specific intermolecular interactions involving either the acylating- or leaving-group regions of the CI2-binding loop, it was necessary to verify that no larger structural repercussions had been introduced by the mutations. To that end, X-ray structures, ranging from 1.3 to 1.7 Å resolution, were obtained for complexes of subtilisin BPN′ with all of the CI2 mutants described. A summary of the data collection and refinement statistics is presented in Table 2. A global structural comparison indicates that no gross changes in the CI2 backbone structure have been introduced

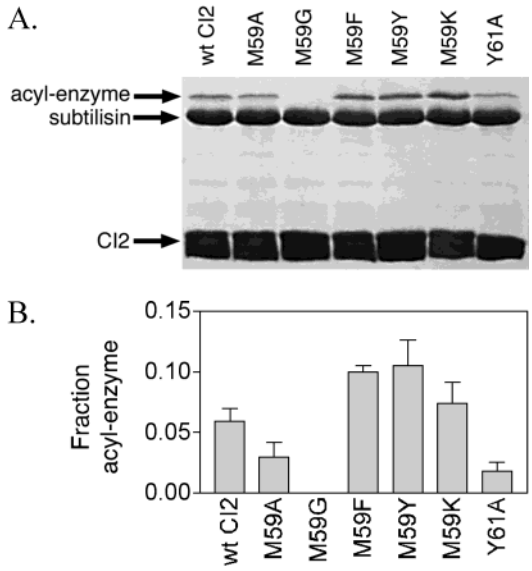

FIGURE 3: Formation of acyl−enzyme between subtilisin BPN′ and CI2 mutants. (A) Subtilisin BPN′ samples (8 μg) were incubated with an excess of wild-type or mutant CI2, allowing formation of an equilibrium population of the acyl−enzyme species, acidified to quench enzyme activity and trap the acyl−enzyme, and then analyzed by SDS−PAGE; a representative gel is shown. (B) Fraction of the total enzyme represented by the acyl−enzyme was estimated from gels. Error bars represent the standard error of the mean for four or more determinations on replicate gels.

by the mutations (Figure 4A). Superpositions were based on the α-carbon positions of all residues of subtilisin minus the His tag, plus the residues of the CI2-binding loop (residues I56−I61). The residues of the CI2 core were not used in superpositioning, because the junction between the CI2 core and binding loop displays a degree of flexibility, with slight hinge angle variations between the mutant complexes. Average root-mean-square (rms) deviations of α-carbon positions, for the residues used in superpositioning, range from 0.069 Å (between the wild-type and M59A complexes) to 0.117 Å (between the wild-type and M59F complexes). The structural differences between the wild-type complex in two different crystal forms, resulting from different crystal packing interactions, are actually greater than the differences among mutant complexes; the two wild-type structures show an average rms deviation of the α-carbon positions, for the residues used in superpositioning, of 0.271 Å (Figure 4B). The $P2_12_12_1$ (*3*) and $P6_522$ crystal forms differ markedly in the CI2 hinge angle, by 8.1°, and many peripheral loops of subtilisin display subtle displacements. The subtilisin His tag takes on completely different conformations in each of the two crystal forms, indicating that it is most likely unstructured in solution.

Structural comparison of the walls of the S_1 specificity cleft of subtilisin in the P_1 mutant complexes reveals only a small degree of adjustment in the backbones of residues that form the binding subsite, to accommodate the mutated CI2 side chains (Figure 5A). The largest backbone displacements are seen in the complexes with M59Y and M59F, to accommodate these larger aromatic side chains. Maximal displacements relative to the native structure are seen at subtilisin residues 127−128 (up to 0.73 Å) and 166 (0.5 Å), while residues 155−156 show a more subtle displacement (0.25 Å). *B*-factor analysis gives an indirect indication of the relative flexibility of active-site residues between the

Table 2: Summary of Data Collection and Refinement Statistics

	wild type	M59K	M59Y	M59F	M59A	M59G	Y61A	M59K pH 9
PDB ID	1TM1	1TM3	1TM7	1TMG	1TM5	1TM4	1TO1	1TO2
cell (Å)								
a = b	93.72	94.20	94.15	94.16	93.78	94.10	94.07	93.67
c	185.85	187.62	186.42	185.32	185.76	186.81	185.77	185.92
resolution (Å)	1.70	1.57	1.59	1.67	1.45	1.70	1.68	1.30
unique reflections	52 791	68 455	66 113	56 854	81 746	54 020	55 676	109 999
completeness (%)	98.2	99.0	99.8	99.8	95.6	99.4	99.4	98.4
multiplicity	4.8	19.4	9.8	17.6	2.3	17.6	4.7	4.1
$I/SD^{a,b}$	13.9 (3.5)	24.3 (3.9)	18.0 (3.5)	20.8 (3.1)	9.7 (2.3)	19.7 (2.5)	10.3 (2.4)	13.2 (2.3)
R_{merge} (%)^{b,c}	6.8 (42)	8.9 (68)	8.1 (48)	11.5 (69)	4.3 (28)	11.2 (93)	9.9 (61)	5.3 (49)
R_{cryst} (%)^{d}	15.1	16.6	15.5	14.9	16.1	15.8	15.6	16.8
R_{free} (%)	18.2	18.4	17.5	17.4	17.9	18.3	18.2	18.3
rmsd bonds (Å)^{e}	0.020	0.018	0.020	0.020	0.019	0.020	0.019	0.019
rmsd angles (deg)^{e}	1.794	1.729	1.815	1.768	1.880	1.731	1.728	1.915
protein average B (Å^2)	16.0	15.2	17.1	14.7	15.0	19.4	16.6	12.6
water average B (Å^2)	34.4	30.7	33.5	33.0	32.7	34.8	34.7	28.3

[a] I = intensity, and SD = standard deviation. [b] Outer shell values are given in parentheses. [c] $R_{merge} = \sum|I - \langle I\rangle|/\sum I \times 100\%$. [d] $R_{cryst} = \sum|F_{obs} - F_{calc}|/\sum F_{obs} \times 100\%$. [e] rms deviations from the ideal geometry.

mutant complexes (Figure 5B). The M59G mutant has noticeably higher B factors, indicative of greater flexibility, in the CI2 backbone residues 59 and 60 flanking the scissile bond, in subtilisin residues 125, 153, and 154, comprising the adjacent walls of the S_1 cleft, and in the subtilisin Ser 221 side chain. The active-site features, including the catalytic triad and the CI2-binding loop P_1 and P_1' residues, superpose almost perfectly for all mutants, and the complexes retain the ideal geometry for nucleophilic attack of Ser 221 on the scissile bond (*3*).

Organized water molecules within the S_1 cleft of subtilisin play a role in enzyme−inhibitor recognition at the binding interface. The most significant structural effects of the CI2 P_1 residue mutations involve modulation of the solvent structure. The larger aromatic P_1 side chains of M59Y and M59F extend more deeply into the S_1 cleft, excluding two ordered water molecules, S57 and S189; in these structures, a single, completely buried water, S35, remains at the back of the cleft. The smaller or absent side chains of M59A and M59G result in the addition of ordered water molecules to the hydrogen-bonded solvent network in the S_1 cleft; M59A sees the addition of S420, while M59G has two added waters, S420 and S421 (Figure 6). The absence of any greater structural consequences of the P_1 mutations allows us to clearly attribute the observed increases in K_i and k_{cat} for the mutants directly to the P_1 side-chain replacement and solvent restructuring in the S_1 cleft.

The structure of the Y61A complex similarly confirms that the functional effects of this mutation, reduced binding affinity and increased hydrolysis, result solely from lost favorable contacts between CI2 Tyr 61 and subtilisin Phe 189. In the wild-type complex, the two aromatic side chains form an offset ring-stacking interaction, in which the ring planes are parallel to each other and separated by approximately 3.5 Å. The structure of the Y61A complex is marked by the replacement of the tyrosine side chain with two ordered water molecules, S388 and S492, with almost no change in the surrounding protein structure (Figure 7), echoing our findings with the P_1 mutants. The catalytic triad and the CI2-binding loop P_1 and P_1' residues also superpose closely with those of the wild-type complex, retaining the ideal orientation for nucleophilic attack of Ser 221 on the scissile bond (*3*).

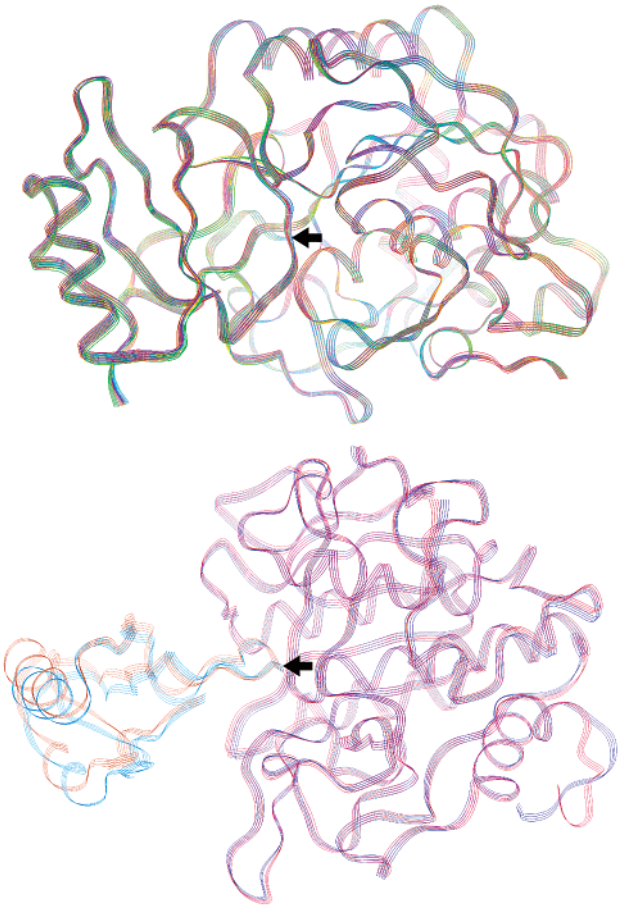

FIGURE 4: Superpositions of subtilisin BPN′/CI2 complexes. (A) Ribbon traces representing subtilisin complexes with wild-type CI2 (red), M59K (orange), M59Y (yellow), M59F (green), M59A (cyan), M59G (blue), and Y61A (purple). The CI2 binding loop lies roughly in the plane of the page, with the black arrow indicating the location of the scissile bond. (B) Ribbon traces of wild-type complexes in space groups $P2_12_12_1$ [subtilisin in red, and CI2 in orange; PDB ID 1LW6 (*3*)] and $P6_522$ (subtilisin in dark blue, and CI2 in medium blue). This view is rotated such that the CI2-binding loop is roughly perpendicular to the page, to highlight the hinge angle displacement between complexes. The black arrow again indicates the scissile bond. The C-terminal His tag of subtilisin is located in the lower right corner of the illustration. All superpositions were based on the α carbons of all enzyme residues minus the His tag plus the CI2-binding loop residues 56−61.

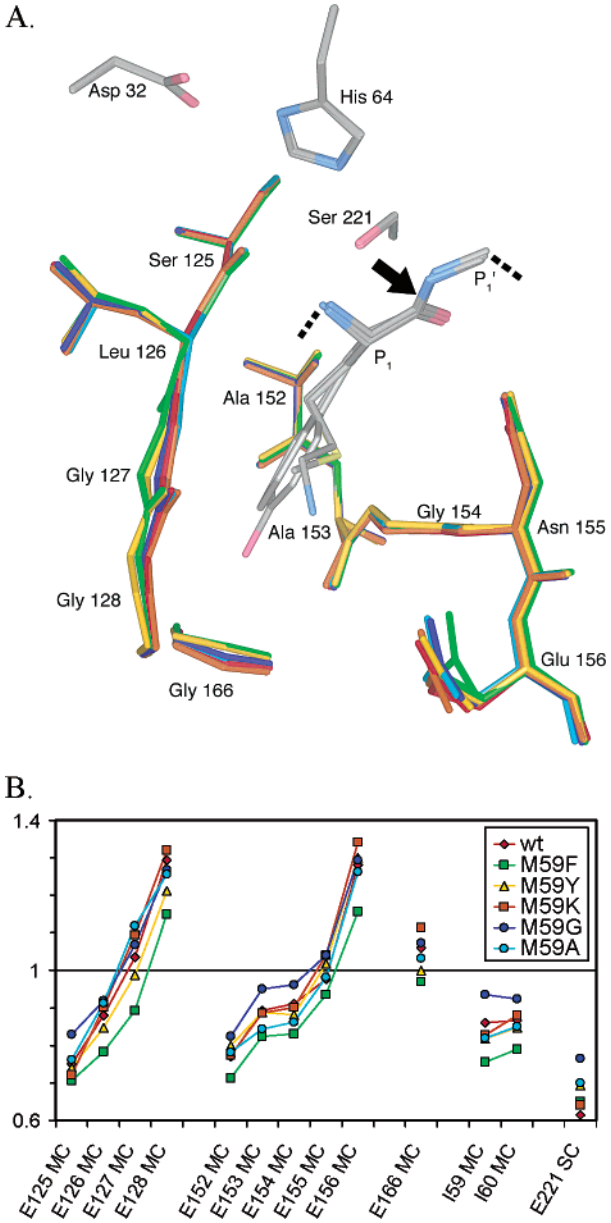

FIGURE 5: Active site and S_1-binding cleft of subtilisin BPN′ in complex with P_1 variants of CI2. (A) Residues of subtilisin forming the S_1 pocket walls in the various complexes are shown in bright colors: red (wild-type CI2), orange (M59K), yellow (M59Y), green (M59F), cyan (M59A), and blue (M59G). For all complexes, the P_1 and P_1' residues of CI2 and the catalytic triad residues of subtilisin are shown in pale colors, where carbons are gray, nitrogens are pale blue, oxygens are pink, and sulfurs are pale yellow. The dotted lines indicate the continuation of the CI2 backbone, and the black arrow indicates the scissile bond. (B) Average *B* factors are plotted for the main-chain (MC) atoms comprising the walls of the S_1 cleft of subtilisin, the main-chain (MC) atoms of CI2 P_1 and P_1' residues 59 and 60, and the side-chain (SC) atoms of the subtilisin nucleophilic serine, Ser 221. Raw *B* factors for each structure have been normalized with division by the average protein *B* factor for that structure, such that a value of 1 corresponds to the average protein *B* factor for that structure.

The M59G Mutant: Variation on the Clogged Gutter Inhibition Mechanism. M59G is the most weakly bound of the P_1 mutants. It would be expected to be the most rapidly hydrolyzed of the P_1 mutants according to the binding/hydrolysis correlation (Figure 2), because the weaker enzyme−inhibitor association should make the interface more accessible to the hydrolytic water at the acyl−enzyme stage and

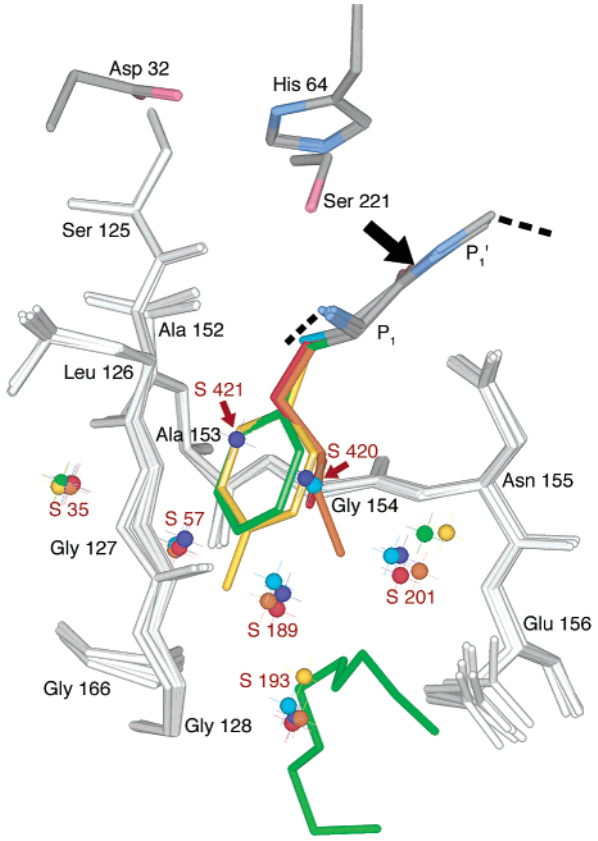

FIGURE 6: P_1 residue side chain and solvent positioning in the S_1-binding cleft. P_1 residue side chains and solvent molecules are shown in red (wild-type CI2), orange (M59K), yellow (M59Y), green (M59F), cyan (M59A), and blue (M59G). Water molecules present in some or all of the structures are labeled in red. The green chain at the bottom of the figure represents a PEG molecule that replaces water S193 in the M59F structure. The backbone atoms of CI2 P_1 and P_1' residues and the side chains of the subtilisin catalytic triad residues are colored gray (carbon atoms), pale blue (nitrogen atoms), and pink (oxygen atoms), while residues of subtilisin forming the S_1 cleft walls are shown in white, for all structures. The dotted lines indicate the continuation of the CI2 backbone, and the black arrow indicates the scissile bond.

should lead to a more rapid product release. The changes in the scissile bond region dynamics implied by the *B*-factor analysis of this mutant would likewise suggest greater susceptibility to hydrolysis and dissociation. However, the M59G mutant is as resistant to hydrolysis as wild-type CI2, causing it to appear as a major outlier in the correlation between binding and hydrolysis (Figure 2). A clue to the explanation is found in the gel analysis of acyl−enzyme formation. No acyl−enzyme species was detected for the M59G mutant, suggesting that for this mutant, the primary barrier to proteolysis occurs not at the deacylation stage but earlier. Apparently, the Michaelis complex proceeds less rapidly to the acyl−enzyme, resulting in little buildup of an acyl−enzyme population.

The reason for this alteration in the mechanism of inhibition is not apparent from the structure of the M59G complex; the positioning of the subtilisin serine nucleophile relative to the CI2 scissile bond is unchanged in the mutant structure. We are left to speculate that the favorable interactions between a P_1 side chain and the S_1-binding cleft play a much larger role in stabilizing the tetrahedral transition state and acyl−enzyme intermediate than they do in the

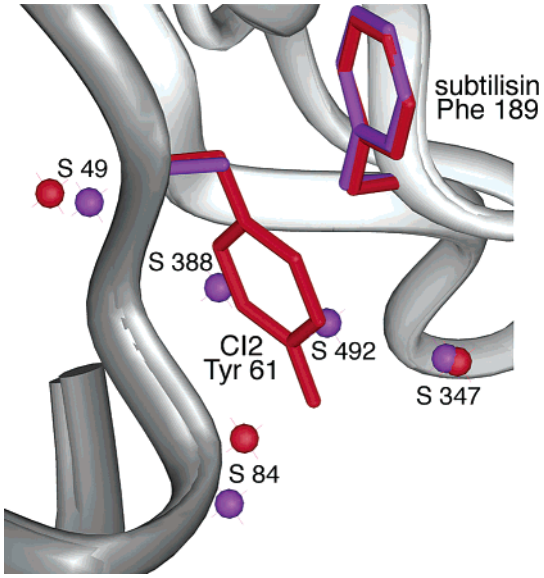

FIGURE 7: Detail of the aromatic side chains and solvent structure at the enzyme−inhibitor interface of subtilisin BPN′ in complex with wild-type CI2 and the Y61A mutant. Side chains of CI2 residue 61, subtilisin Phe 189, and proximal solvent molecules are shown in red (wild-type CI2) and purple (Y61A). A white ribbon represents the subtilisin backbone, and a gray ribbon represents the CI2 backbone.

Table 3: Kinetic Constants for Hydrolysis of Succinyl-Ala-Ala-Pro-[X]-*p*-nitroanaline Substrates by Subtilisin BPN′[a]

P_1 residue	k_{cat} (s^{-1})	K_M (M)	k_{cat}/K_M (M^{-1} s^{-1})
Met	13	9.0×10^{-5}	1.4×10^{5}
Gly	0.003	1.2×10^{-4}	25
Ala	1.9	1.5×10^{-4}	1.4×10^{4}
Lys	30	7.5×10^{-4}	4.0×10^{4}
Tyr	25	1.8×10^{-5}	1.4×10^{6}
Phe	50	1.4×10^{-4}	3.6×10^{5}

[a] Data taken from the work of Wells, Estell, and colleagues (*8*, *9*).

Michaelis complex, and that the absence of a P_1 side chain in the M59G mutant is much more destabilizing to the tetrahedral transition state and acyl−enzyme intermediate than it is to the Michaelis complex. This mirrors the situation with subtilisin and a series of peptide succinyl-Ala-Ala-Pro-[X]-*p*-nitroanaline substrates, where K_M was minimally increased for the P_1 glycine substrate relative to good substrates, indicating a modest reduction in binding, while k_{cat} was reduced by over 3 orders of magnitude (Table 3). The literature contains other examples of serine proteases, notably trypsin (*28*) and *Streptomyces griseus* protease 1 (*29*), in which P_1 specificity is expressed primarily through k_{cat} rather than K_M, revealing a general importance of the substrate P_1 residue in stabilizing the transition state. Similarly, for the *Saccharomyces cerevisiae* protease Kex2, the enzyme−substrate interaction at P_1 is used almost entirely for transition-state stabilization of the acylation reaction (*30*).

The M59K Mutant: Significance of Electrostatic Interactions. The Met and Lys P_1 side chains and associated water molecules superpose almost perfectly (Figure 8), allowing us to attribute the 6-fold reduction in the binding affinity solely to the introduction of the charged lysine amino group. This charged group has a deleterious effect on the binding affinity despite the fact that it is located near the mouth of

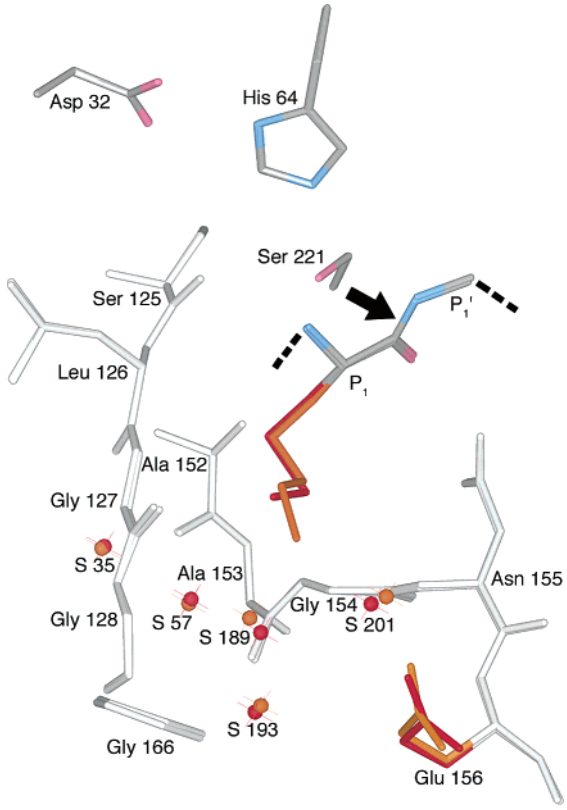

FIGURE 8: Comparison of the Met and Lys P_1 side chains and solvent structure in the S_1 pocket of subtilisin BPN′. P_1 residue side chains, Glu 156 side chains, and water molecules are shown in red (wild-type C12) and orange (M59K). The backbone atoms of C12 P_1 and P_1′ residues and the side chains of the subtilisin catalytic triad residues are colored gray (carbon atoms), pale blue (nitrogen atoms), and pink (oxygen atoms), while residues of subtilisin forming the S_1 pocket walls are shown in white, for both structures. The dotted lines indicate the continuation of the C12 backbone, and the black arrow indicates the scissile bond.

the broad binding cleft and forms hydrogen bonds with two water molecules, S189 and S201.

It has been pointed out in the literature that Lys is an alternative preferred P_1 residue for subtilisin BPN′, although not for subtilisin Carlsberg, as the result of electrostatic interaction between a P_1 Lys residue and the carboxylate anion of Glu 156 in the S_1-binding cleft of subtilisin BPN′ (*10*, *11*). Crystallography of a covalent adduct between subtilisin BPN′ and a putative tetrahedral intermediate analogue, Phe-Ala-Lys-chloromethyl ketone, revealed an ion pair 3.1 Å in length (*10*), and subtilisin mutagenesis studies showed the electrostatic interaction between Glu 156 and P_1 Lys to favor catalysis, lowering the transition-state free energy by 1.8 kcal/mol (*11*).

Our structure of the complex between subtilisin BPN′ and the M59K CI2 mutant allows us to contrast a Michaelis complex structure with that of the tetrahedral intermediate analogue; the validity of our complex as a model of the Michaelis complex is confirmed by the rapid acylation that we observe. The M59K mutant structure reveals that, in the Michaelis complex, the P_1 Lys amine and the Glu 156 carboxylate are separated by 4.3 Å. A water molecule, S201, is 2.9 Å from the P_1 Lys amine and 2.3 Å from the Glu 156 carboxylate and could potentially bridge the electrostatic interaction; however, S201 has a relatively diffuse electron density and a *B* factor slightly higher than the average solvent

B factor for this structure. These facts, combined with the solvent-exposed position of the potential ion pair and the observed deleterious effect of the M59K mutation on CI2 binding, make a strong electrostatic interaction unlikely in the Michaelis complex. We eliminated the possibility that the structural variations in our complex might be an artifact of the low crystallization pH by repeating the structure determination on a crystal that had undergone a soak at pH 9; the high pH structure showed no differences.

Our findings, when taken together with previous studies (*10*, *11*), suggest that the electrostatic interaction between Glu 156 of subtilisin BPN′ and a substrate P_1 Lys residue is insignificant in the Michaelis complex but becomes important in the transition state and tetrahedral intermediate. Progress along the reaction path towards the transition state may be marked by reorganization of solvent and movement of the charged side chains toward each other, which may serve as a mechanism of transition-state stabilization. Further evidence for this suggestion is found in kinetic studies of peptide substrate hydrolysis by subtilisin BPN′; succinyl-Ala-Ala-Pro-Lys-*p*-nitroanaline is bound at an order of magnitude more weakly than the equivalent methionine substrate but has a greater k_{cat} (Table 3), indicating that the charged P_1 residue contributes more to transition-state stabilization than initial binding.

Subtilisin S_1 Cleft Discrimination. The data reported here for binding affinities of subtilisin BPN′ for the CI2 P_1 mutants, in combination with the high-resolution structures of the complexes, provide new insight into the specificity of subtilisin and the energetic consequences of replacing buried hydrophobic surface area with ordered solvent at a binding interface. Although the subtilisin S_1 binding cleft is often described as ideal for accepting large hydrophobic residues, there appear to be only minor energetic consequences for the replacement of the hydrophobic contacts present when Phe, Tyr, or Met is bound with ordered waters in a hydrogen-bonded network, in the case of a smaller or absent P_1 side chain. Even when the bulky hydrophobic P_1 residues are bound, a buried water molecule, S35, remains at the bottom of the S_1-binding cleft, involved in a network of hydrogen bonds at the enzyme−inhibitor interface. Surprisingly, M59A binds with similar affinity to M59F, revealing that the S_1 cleft shows little preference for the aromatic side chain over the 3 water molecules that replace it in the M59A mutant. Involvement of bound waters in molecular recognition of variant P_1 residues has been noted for other protease−inhibitor pairs, such as for the complex of *Streptomyces griseus* proteinase B with the turkey ovomucoid inhibitor third domain (OMTKY) (*31*) and the complex of bovine trypsin with BPTI (*32*).

Generality of the Clogged Gutter Mechanism. While our studies have been limited to the interaction between subtilisin BPN′ and chymotrypsin inhibitor 2, a comparison of the active sites of many protease−inhibitor complexes reveals that they share a characteristic inhibitor backbone conformation at the enzyme interface and nearly identical geometry for approach of the serine nucleophile to the scissile bond (*3*). This striking structural similarity suggests that the subtilisin BPN′/CI2 complex may be representative of other protein protease inhibitor complexes with respect to the ease of acyl−enzyme formation (*3*). It is tempting to speculate that retention of the leaving-group peptide, favoring religation of the inhibitor scissile bond, may also be a common feature, giving the clogged gutter mechanism a central role in the function of the classic serine protease inhibitors. However, alternative interpretations could also be considered.

For a number of the most intensely studied protease inhibitors, the process of enzyme binding, cleavage, and dissociation has been shown to be fully reversible, resulting in an eventual equilibrium between the intact and cleaved inhibitor, with an equilibrium constant near unity (*1*, *33*). For OMTKY3, Ardelt and Laskowski presented evidence that subtilisin Carlsberg resynthesizes the intact inhibitor from the cleaved form much more rapidly than chymotrypsin or elastase (*34*). It is possible that the subtilisins but not the chymotrypsin family of proteases create a uniquely favorable environment for religation of the cleaved reactive site bond, explaining both our data and that of Ardelt and Laskowski. The pervasiveness of the clogged gutter mechanism with enzymes and inhibitors beyond subtilisin BPN′ and CI2 remains to be experimentally explored.

Summary of Conclusions. The previously proposed clogged gutter mechanism of CI2 inhibition (*3*), in which turnover following acylation is slowed by retention of the leaving group in the active site and promotion of inhibitor religation, suggested a testable hypothesis. While the acylating residues are more critical for ordinary substrates, where acylation is rate-limiting, we predicted that leaving-group determinants would be more critical for implementing CI2 inhibition. We found that mutation of Tyr 61 of CI2, which forms the most significant leaving-group contacts with the enzyme, did indeed interfere with the inhibitory function to a greater extent than the mutation of Met 59, the P_1 residue that forms the strongest enzyme contacts on the acylating side of the scissile bond. We found that a correlation exists between CI2 hydrolysis and binding, which is completely consistent with rate-determining deacylation and product dissociation. Significantly, CI2 hydrolysis did not correlate with either k_{cat} or k_{cat}/K_m for peptide substrates featuring the same P_1 residues (data in Table 3), further emphasizing that CI2 hydrolysis is not slowed at the acylation step, which is rate-limiting for the peptide substrates (*5*). High-resolution crystal structures of the mutant complexes, which show no large shifts in backbone conformation, allowed us to attribute the mutational effects on binding and hydrolysis directly to the loss of very specific intermolecular interactions and reorganization of solvent molecules.

Our data also provide fortuitous insight into the catalytic mechanism of subtilisin BPN′. In the M59G CI2 mutant, hydrolysis appears to be slowed at the acylation step, despite optimal orientation of the scissile bond and catalytic triad; we interpret this as evidence for the importance of the P_1 side chain for transition-state stabilization during acylation. Structural data from the M59K CI2 mutant likewise imply a role for this residue in transition-state stabilization, because electrostatic interactions known to be of importance in catalysis were not in evidence in the ground-state Michaelis complex structure and must therefore evolve along the reaction coordinate.

ACKNOWLEDGMENT

We thank Susan Marqusee for use of the Bio-Logic SFM-400/Q quench-flow instrument and James Holton and

George Meigs for technical assistance with X-ray data collection. We also thank the referees for their insightful comments and helpful suggestions.

REFERENCES

1. Laskowski, M., Jr., and Kato, I. (1980) Protein inhibitors of proteinases, *Annu. Rev. Biochem. 49*, 593−626.
2. Bode, W., and Huber, R. (1992) Natural protein proteinase inhibitors and their interaction with proteinases, *Eur. J. Biochem. 204*, 433−451.
3. Radisky, E. S., and Koshland, D. E., Jr. (2002) A clogged gutter mechanism for protease inhibitors, *Proc. Natl. Acad. Sci. U.S.A. 99*, 10316−10321.
4. Philipp, M., and Bender, M. L. (1983) Kinetics of subtilisin and thiolsubtilisin, *Mol. Cell. Biochem. 51*, 5−32.
5. Wells, J. A., Cunningham, B. C., Graycar, T. P., and Estell, D. A. (1986) Importance of hydrogen-bond formation in stabilizing the transition state of subtilisin, *Philos. Trans. R. Soc. London, Ser. A 317*, 415−423.
6. Gron, H., Meldal, M., and Breddam, K. (1992) Extensive comparison of the substrate preferences of two subtilisins as determined with peptide substrates which are based on the principle of intramolecular quenching, *Biochemistry 31*, 6011−6018.
7. Perona, J. J., and Craik, C. S. (1995) Structural basis of substrate specificity in the serine proteases, *Protein Sci. 4*, 337−360.
8. Estell, D. A., Graycar, T. P., Miller, J. V., Powers, D. B., Burnier, J. P., Ng, P. G., and Wells, J. A. (1986) Probing steric and hydrophobic effects on enzyme−substrate interactions by protein engineering, *Science 233*, 659−663.
9. Wells, J. A., Cunningham, B. C., Graycar, T. P., and Estell, D. A. (1987) Recruitment of substrate-specificity properties from one enzyme into a related one by protein engineering, *Proc. Natl. Acad. Sci. U.S.A. 84*, 5167−5171.
10. Poulos, T. L., Alden, R. A., Freer, S. T., Birktoft, J. J., and Kraut, J. (1976) Polypeptide halomethyl ketones bind to serine proteases as analogs of the tetrahedral intermediate, *J. Biol. Chem. 251*, 1097−1103.
11. Wells, J. A., Powers, D. B., Bott, R. R., Graycar, T. P., and Estell, D. A. (1987) Designing substrate specificity by protein engineering of electrostatic interactions, *Proc. Natl. Acad. Sci. U.S.A. 84*, 1219−1223.
12. Otzen, D. E., and Fersht, A. R. (1999) Analysis of protein−protein interactions by mutagenesis: Direct versus indirect effects, *Protein Eng. 12*, 41−45.
13. Wells, J. A., Ferrari, E., Henner, D. J., Estell, D. A., and Chen, E. Y. (1983) Cloning, sequencing, and secretion of *Bacillus amyloliquefaciens* subtilisin in *Bacillus subtilis*, *Nucleic Acids Res. 11*, 7911−7925.
14. Radisky, E. S., King, D. S., Kwan G., and Koshland, D. E., Jr. (2003) The role of the protein core in the inhibitory power of the classic serine protease inhibitor, chymotrypsin inhibitor 2, *Biochemistry 42*, 6484−6492.
15. Longstaff, C., Campbell, A. F., and Fersht, A. R. (1990) Recombinant chymotrypsin inhibitor 2: Expression, kinetic analysis of inhibition with α-chymotrypsin and wild-type and mutant subtilisin BPN′, and protein engineering to investigate inhibitory specificity and mechanism, *Biochemistry 29*, 7339−7347.
16. Holton, J., and Alber, T. (2004) Automated protein crystal structure determination using ELVES, *Proc. Natl. Acad. Sci. U.S.A. 101*, 1537−1542.
17. Leslie, A. G. W. (1992) Recent changes to the MOSFLM package for processing film and image plate data, *Joint CCP4+ESF-EAMCB Newsletter on Protein Crystallography 26*.
18. Collaborative Computational Project Number 4 (1994) The CCP4 suite: Programs for protein crystallography, *Acta Crystallogr., Sect. D 50*, 760−763.
19. Kissinger, C. R., Gehlhaar, D. K., and Fogel, D. B. (1999) Rapid automated molecular replacement by evolutionary search, *Acta Crystallogr., Sect. D 55*, 484−491.
20. Jones, T. A., Zou, J. Y., Cowan, S. W., and Kjeldgaard, M. (1991) Improved methods for building protein models in electron density maps and the location of errors in these models, *Acta Crystallogr., Sect. A 47*, 110−119.
21. Murshudov, G. N., Vagin, A. A., and Dodson, E. J. (1997) Refinement of macromolecular structures by the maximum-likelihood method, *Acta Crystallogr., Sect. D 53*, 240−255.
22. Perrakis, A., Morris, R., and Lamzin, V. S. (1999) Automated protein model building combined with iterative structure refinement, *Nat. Struct. Biol. 6*, 458−463.
23. Hooft, R. W. W., Vriend, G., Sander, C., and Abola, E. E. (1996) Errors in protein structures, *Nature 381*, 272−272.
24. Fauman, E. B., Rutenber, E. E., Maley, G. F., Maley, F., and Stroud, R. M. (1994) Water-mediated substrate/product discrimination: The product complex of thymidylate synthase at 1.83 Å, *Biochemistry 33*, 1502−1511.
25. Perona, J. J., Craik, C. S., and Fletterick, R. J. (1993) Locating the catalytic water molecule in serine proteases, *Science 261*, 620−620.
26. Farber, G. K. (1999) Crystallographic analysis of solvent-trapped intermediates of chymotrypsin, *Methods Enzymol. 308*, 201−215.
27. Hedstrom, L. (2002) Serine protease mechanism and specificity, *Chem. Rev. 102*, 4501−4524.
28. Gráf, L., Jancsó, Á., Szilágyi, L., Hegyi, G., Pintér, K., Náray-Szabó, G., Hepp, J., Medzihradszky, K., and Rutter, W. (1988) Electrostatic complementarity within the substrate-binding pocket of trypsin, *Proc. Natl. Acad. Sci. U.S.A. 85*, 4961−4965.
29. Bauer, C.-A. (1978) Active centers of *Streptomyces griseus* protease 1, *Streptomyces griseus* protease 3, and α-chymotrypsin: Enzyme−substrate interactions, *Biochemistry 17*, 375−380.
30. Rockwell, N. C., and Fuller, R. S. (2001) Differential utilization of enzyme−substrate interactions for acylation but not deacylation during the catalytic cycle of Kex2 protease, *J. Biol. Chem. 276*, 38394−38399.
31. Huang, K., Lu, W., Anderson, S., Laskowski, M., Jr., and James, M. N. G. (1995) Water molecules participate in proteinase-inhibitor interactions: Crystal structures of Leu^{18}, Ala^{18}, and Gly^{18} variants of turkey ovomucoid inhibitor third domain complexed with *Streptomyces griseus* proteinase B, *Protein Sci. 4*, 1985−1997.
32. Helland, R., Otlewski, J., Sundheim, O., Dadlez, M., and Smalås, A. O. (1999) The crystal structures of the complexes between bovine β-trypsin and ten P_1 variants of BPTI, *J. Mol. Biol. 287*, 923−942.
33. Ardelt, W., and Laskowski, M., Jr. (1991) Effect of single amino acid replacements on the thermodynamics of the reactive site peptide bond hydrolysis in ovomucoid third domain, *J. Mol. Biol. 220*, 1041−1053.
34. Ardelt, W., and Laskowski, M., Jr. (1985) Turkey ovomucoid third domain inhibits eight different serine proteases of varied specificity on the same ...Leu^{18}-Glu^{19}... reactive site, *Biochemistry 24*, 5313−5320.
35. Schechter, I., and Berger, A. (1967) On the size of the active site in proteases. I. Papain, *Biochem. Biophys. Res. Commun. 27*, 157−162.

BI048797K